Concurrent Transformation of Copolymer Domain Morphology Induced by the Order−Disorder Transition of Comb Block in Supramolecular Comb−Coil Block Copolymer

Cheng-Si Tsao[†] and Hsin-Lung Chen*[,‡]

Institute of Nuclear Energy Research, Longtan, Taoyuan 325, Taiwan, R.O.C., and Department of Chemical Engineering, National Tsing Hua University, Hsin-Chu 30013, Taiwan, R.O.C.

Received July 19, 2004; Revised Manuscript Received September 10, 2004

ABSTRACT: An amphiphilic surfactant, dodecylbenzenesulfonic acid (DBSA), was complexed with poly(ethylene oxide) (PEO) block in poly(1,4-butadiene)-*block*-PEO (PB-*b*-PEO) through hydrogen bonding to yield a molecular architecture resembling comb−coil diblock copolymer. For the two binding fractions ($x = 0.5$ and 1.0 with x being the average number of DBSA molecules bound with one PEO monomer unit) studied, the supramolecular comb−coil diblocks exhibited a cylinder-within-lamellae morphology, where the PB cylindrical domains of ca. 28 nm in diameter embedded in the matrix consisting of the lamellar mesophase with the interlamellar distance of ca. 2.9 nm organized by the PEO(DBSA)$_x$ comb blocks. The interdomain distance of PB cylinders was significantly smaller than the fully extended length of the PEO block, indicating that the PEO chains confined within the polar layers in the lamellar mesophase were not fully stretched normal to the interface of PB microdomain; alternatively, they adopted a folded conformation while lying on the lamellar plane to alleviate the entropic penalty of the PB blocks while accommodating the formation of lamellar stacks. The secondary force building up the comb structure allowed the order−disorder transition (ODT) from the lamellar phase to a disordered phase in which the comb structure persisted to be accessed easily. Accompanied with this ODT was a concurrent transformation of the PB domain morphology from cylinder to sphere. This demonstrates that, in addition to the structure-within-structure morphology, the supramolecular comb−coil diblock exhibited a transition-driven transition through which the morphology of the larger scale copolymer domain was switched by the ODT of the smaller scale assembly of the comb block.

Introduction

Polymers with hierarchical structure have been drawing significant interest due to their potential use as functional materials in electrical, optical, and other functionalities.[1−4] The self-organized domains at multiple length scales offer switchlike controls of material functionalities by the relevant order−disorder or order−order transitions.[3,4] Therefore, it becomes important to develop a sufficiently simple way to construct hierarchical structures and to tailor the structural transition temperatures for switching control.

Block copolymers capable of self-assembling to form long-range ordered microdomains are attractive building blocks for hierarchical nanostructures.[5,6] The basic strategy involves the induction of a shorter-length scale assembly within the microdomain or the matrix phase so as to generate a smaller nanostructure coexisting with the larger copolymer domain. This kind of structure-within-structure morphology may be found (although not been emphasized) in crystalline−amorphous diblock copolymers, where the ordered stacking of crystallites within the crystalline domains constitutes the smaller nanostructure.[7] Introducing mesomorphic order into the copolymer domains using comb−coil dibock copolymers offers another pathway toward structures with two distinct length scales. In this case, the larger structure at several tens of nanometers corresponds to the copolymer domains, and the smaller one is usually a lamellar mesophase with a characteristic length of several nanometers organized by the comb blocks.

One advantage of using comb−coil block copolymer as the building block for hierarchical assemblies lies in the relative easiness of synthesizing the comb architecture through a supramolecular approach in which the polymer backbone is grafted with short chain molecules through noncovalent interactions. Amphiphilic surfactants comprising of a polar headgroup and a flexible hydrocarbon chain per molecule are convenient choices for the grafts. In this case, the attachment of the headgroups to the complementary binding sites on the polymer chain via ionic[8−11] or hydrogen bonding yields a comblike supramolecule (or complex) with a polar backbone and nonpolar grafts.[12−16] The polar−nonpolar repulsion between these two units is usually strong enough to induce a microphase separation leading predominantly to a lamellar mesophase consisting of alternating polar and nonpolar layers. The phase transition temperatures of the mesophase may be tailored by the strength of the secondary interaction holding up the comb architecture. Ionic bonding normally results in an order−disorder transition (ODT) temperature (T_{ODT}) well above the thermal decomposition temperature of the system, while ODT becomes accessible prior to thermal degradation for the weaker binding force such as hydrogen bonds.

Recently, Ruokolainen et al.[2,3,17] have adapted the supramolecular approach to construct a series of comb−coil diblock copolymers through hydrogen-bonded complexation of pentadecylphenol (PDP) with poly(4-vinylpyridine) (P4VP) block in polystyrene-*block*-P4VP (PS-*b*-P4VP). The resultant comb−coil systems displayed a rich variety of structure-within-structure morphology in which the P4VP(PDP) comb blocks self-

[†] Institute of Nuclear Energy Research.
[‡] National Tsing Hua University.
* To whom correspondence should be addressed.

10.1021/ma048526h CCC: $27.50
Published on Web 10/30/2004

Table 1. Volume Fractions of PB (f_{PB}) in the PB-*b*-PEO(DBSA)$_x$ Samples under Study

binding fraction in PEO(DBSA)$_x$ block x	f_{PB}
0.0	0.56
0.25	0.28
0.5	0.20
1.0	0.11

assembled into a lamellar structure irrespective of the morphology of the larger PS domain. This lamellar mesophase underwent an ODT at elevated temperatures, but this transition did not affect the morphology of the copolymer domains. When the temperature was much higher than the T_{ODT}, PDP molecules decoupled from the P4VP blocks, and a fraction of them diffused into the PS phase, which then induced a morphological transition of the P4VP-containing domains from lamellae to cylinder due to effective increase of the volume fraction of PS-containing domains.

In this study, we present a new comb−coil diblock copolymer formed by hydrogen-bonded complexation of an amphiphilic surfactant, dodecylbenzenesulfonic acid (DBSA), with the poly(ethylene oxide) (PEO) block in a poly(1,4-butadiene)-*block*-PEO (PB-*b*-PEO). The hydrogen bonding arises from the favorable interaction between the sulfonic acid headgroup in DBSA and the lone-pair electrons of the ether linkage in PEO. The structure-within-structure morphology and the phase transitions of the PB-*b*-PEO(DBSA)$_x$ supramolecules (with x denoting the average number of DBSA molecules bound with an EO monomer unit) are systematically investigated using small-angle X-ray scattering (SAXS) and transmission electron microscopy (TEM). It will be demonstrated that the morphology of the PB microdomain is strongly influenced by the structure of the PEO(DBSA)$_x$ phase tailored by the binding fraction of DBSA on PEO block and temperature. In this case, the system exhibits a "transition-driven transition" where a transformation of the larger scale copolymer domain morphology is induced concurrently by the ODT of the smaller scale lamellar mesophase. This is distinguished from the PS-*b*-P4VP(PDP) system in which the transition of copolymer domain morphology occurred significantly above the T_{ODT} of the lamellar phase.

Experimental Section

Materials and Sample Preparation. The PB-*b*-PEO was acquired from Polymer Source, Inc. M_n of PB and PEO blocks was 11 800 and 11 000, respectively, which prescribed the volume fraction of PB $f_{PB} = 0.56$. The surfactant DBSA (soft type) was obtained from Tokio Kasei, Tokyo, Japan. This material had a purity of 90%, and the remaining impurity consisted of different chain lengths and branches: $(C_nH_{2n+1})(C_mH_{2m+1})CHPhSO_3H$, with $n + m + 1 = 10$, ..., 14. Both materials were dried in vacuo at 60 °C for 12 h before use. PB-*b*-PEO(DBSA)$_x$ complexes were prepared by dissolving PB-*b*-PEO and DBSA in chloroform followed by evaporating most solvent at room temperature. The samples were finally dried in vacuo for more than 2 h to remove the residual solvent. The composition of the complex is denoted by the binding fraction, x, which expresses the average number DBSA molecules bound with an EO monomer unit. Table 1 summarizes the volume fractions of the PB phase in the PB-*b*-PEO(DBSA)$_x$ samples under study.

SAXS Measurement. SAXS measurements were conducted with samples equilibrated at a series of temperatures, i.e., 25, 40, 50, 60, and 70 °C. The X-ray source was an 18 kW rotating anode X-ray generator (Rigaku) equipped with a Cu target. The incident X-ray beam was monochromated by a graphite crystal and collimated subsequently by a set of three pinholes, making smearing effects negligible. The scattering intensity profiles were detected by a 2-D position-sensitive detector (ORDELA 2201X model) with 256 × 256 pixels (active area 20 × 20 cm^2, about 1 mm resolution). The sample-to-detector distance was varied from 4 to 2 m to cover sufficient scattering vector range for structural characterization. The intensity was finally corrected for background and pixel sensitivity, placed on an absolute level using a calibrated secondary standard and circularly averaged to yield the scattered intensity $I(q)$ as a function of the wave vector q, where $q = (4\pi/\lambda)\sin(\theta/2)$ (θ is the scattering angle).

TEM Experiment. The real-space morphology of PB-*b*-PEO(DBSA) was observed by a JEM-2000EX II transmission electron microscope operated at 100 kV. The film specimens were microtomed at −95 °C using a Reichert Ultracut E low-temperature sectioning system. The ultrathin sections were picked onto the copper grids coated with carbon-supporting films followed by staining by exposure to the vapor of 2% osmium tetraoxide (OsO_4) solution for 2 h. OsO_4 is a preferential staining agent for PB blocks, so the PB phase appears dark in the TEM micrographs.

Results and Discussion

Samller Scale Assembly of PEO(DBSA)$_x$ Comb Block. Our previous study of the complexes of PEO homopolymer (h-PEO) with DBSA has demonstrated that the comb supramolecules self-assembled into a lamellar mesophase with the interlamellar distance (D) of ca. 3 nm.[18] Since this interlamellar distance is only a few angstroms larger than that of the lamellar phase organized by neat DBSA, the PEO chains within the polar layers must be highly compressed, where the conformational freedom in the direction normal to the lamellar interface is strongly restricted. The T_{ODT} of the transition from the lamellar mesophase to a disordered phase in which the comb architecture still persisted increased monotonically with increasing binding fraction. In the disordered state the characteristic concentration fluctuations of the comb supramolecules gave rise to a broad correlation hole peak in the corresponding SAXS profile.

In contrast to h-PEO(DBSA)$_x$ complexes, the self-assembly of PEO(DBSA)$_x$ comb blocks in PB-*b*-PEO(DBSA)$_x$ is coupled with the larger scale microphase separation between the comb and the coil blocks. Figure 1 shows the temperature-dependent SAXS profiles in the high-q region (1.1 nm^{-1} < q < 2.9 nm^{-1}) for characterizing the structure organized by PEO(DBSA)$_x$ comb blocks with x of 1.0, 0.5, and 0.25. The peak centering at ca. 2 nm^{-1} for $x = 0.5$ and 1.0 at 25 °C (cf. parts a and b of Figure 1) corresponds to the primary diffraction maximum from the lamellar structure organized by the PEO(DBSA)$_x$ blocks. The second-order peak along with an amorphous halo at $q \sim 13$ nm^{-1} is indeed identifiable in the corresponding wide-angle X-ray scattering (WAXS) pattern, which unambiguously verifies the lamellar structure and the effective suppression of crystallization of PEO in the comb blocks due to complexation with DBSA. The interlamellar distance calculated from Bragg's law is 3.1 and 2.9 nm for $x = 0.5$ and 1.0, respectively. The slightly smaller D at larger x was also found in the corresponding homopolymer complexes and was attributed to the uniform surfactant binding along the PEO chain in that the unbound monomer units distributed evenly along the chain were excluded from the lamellar interface into the core region of the polar layer, which then caused a swelling of interlamellar distance.[12,18]

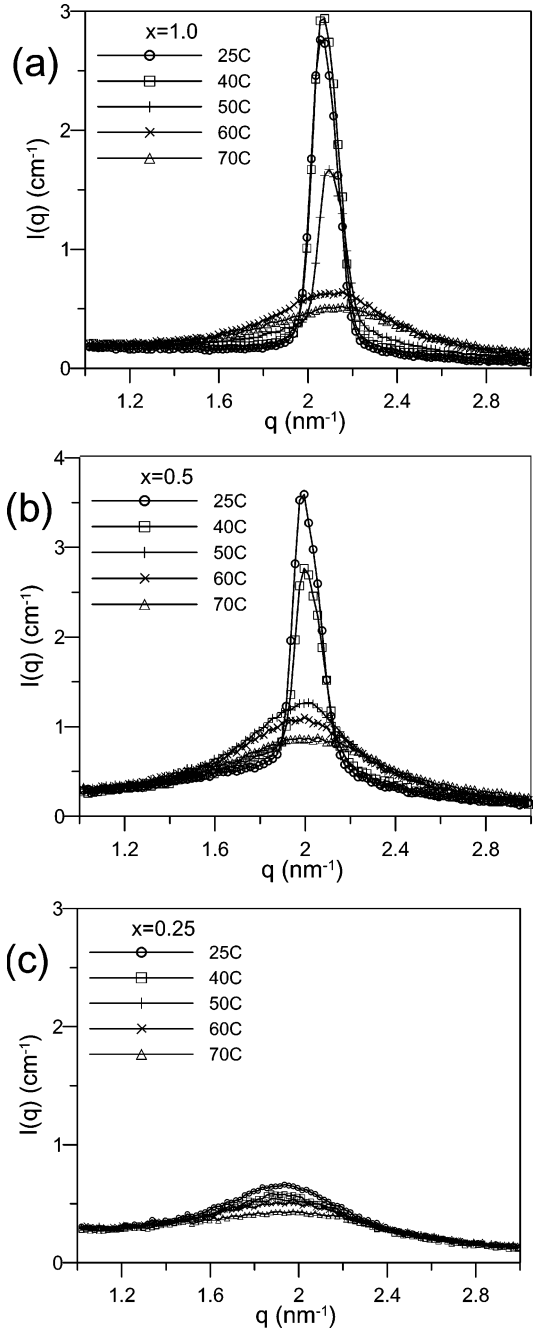

Figure 1. Temperature-dependent SAXS profiles in the high-q region (1.1 $nm^{-1} < q < 2.9$ nm^{-1}) for characterizing the structure organized by PEO(DBSA)$_x$ comb blocks with x of (a) 1.0, (b) 0.5, and (c) 1.0. For $x = 0.5$ and 1.0, the primary scattering peak undergoes a drastic broadening and drop in intensity at elevated temperature, signaling the occurrence of an ODT. The composition of $x = 0.25$ does not form ordered lamellar structure as the corresponding SAXS profiles in (c) display a broad correlation hole peak over the temperature range studied.

For the two binding fractions of $x = 0.5$ and 1.0, the primary scattering peak undergoes a drastic broadening and drop in intensity at elevated temperature, signaling the occurrence of an ODT from lamellar mesophase to a disordered phase in which the persistence of comb structure gives rise to a broad correlation hole peak. The PEO(DBSA)$_x$ block with $x = 0.25$ does not appear to form ordered lamellar structure as the corresponding SAXS profiles in Figure 1c display a broad correlation hole peak over the temperature range studied. In this

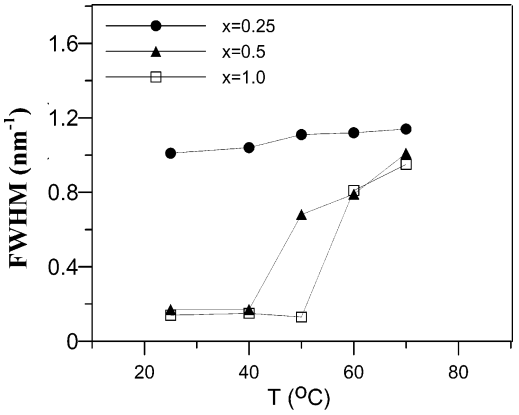

Figure 2. Fwhm of the primary SAXS peak as a function of temperature for estimating the T_{ODT} of the PEO(DBSA)$_x$ blocks with $x = 0.5$ and 1.0.

case, the reduction of polar−nonpolar repulsion on forming the lamellar phase cannot compensate for the entropic losses of PEO and PB blocks (to be discussed below) such that the disordered phase becomes the stable structure.

The T_{ODT}'s of the lamellar mesophases at $x = 0.5$ and 1.0 are assessed from the plot of full width at half-maximum (fwhm) of the SAXS peak vs temperature, as shown in Figure 2. The T_{ODT} thus obtained is ca. 45 and 55 °C for $x = 0.5$ and 1.0, respectively. Decrease of T_{ODT} with decreasing binding fraction was in parallel with that found in the h-PEO(DBSA)$_x$ complexes; nevertheless, the T_{ODT} observed here is about 20 °C lower than that of the homopolymer complex with the same binding fraction.[18] The lower T_{ODT} may be attributed to the intervention of the PB blocks whose conformation is strongly correlated with the highly compressed conformation of PEO blocks in the polar layers of the lamellar mesophase. Let us consider the scenario illustrated in Figure 3a in which the PEO chains lying on the lamellar plane are stretched normal to the copolymer domain interface to maximize the binding with the surfactant headgroups. These stretched PEO chains are densely packed on the lamellar plane unless the number of headgroups on the plane greatly exceeds that of the complementary binding sites on PEO. Such a smectic ordering has been observed for the DNA chains confined between the lipid bilayers in DNA/cationic lipid complexes.[19] Let us assume that the interlamellar distance of ca. 3.0 nm corresponds to the thickness of a monolayer of PEO chains plus that of a DBSA bilayer. In this case, each PB block chain linked with a PEO chain may be considered to be enclosed within a rectangular parallelepiped with a length in the z direction of ca. 3.0 nm and a small width in the x direction prescribed by the interchain distance of the densely packed PEO blocks (cf. Figure 3a). In this case, the conformational freedom of PB blocks in the x direction becomes restricted under the condition of melt incompressibility and hence causes a loss of conformational entropy. The entropic loss can be alleviated if the PEO chains lying on the lamellar plane adopt some folded conformations, as illustrated in Figure 3b. The chain folding effectively increases the cross-sectional area per junction point and thus allows the PB blocks to relax conformationally. This picture is reminiscent of the chain folding in crystalline−amorphous diblock copolymers, where the crystalline block adopts an equilibrium degree of chain folding to enlarge the cross section per junction point to avoid excessive

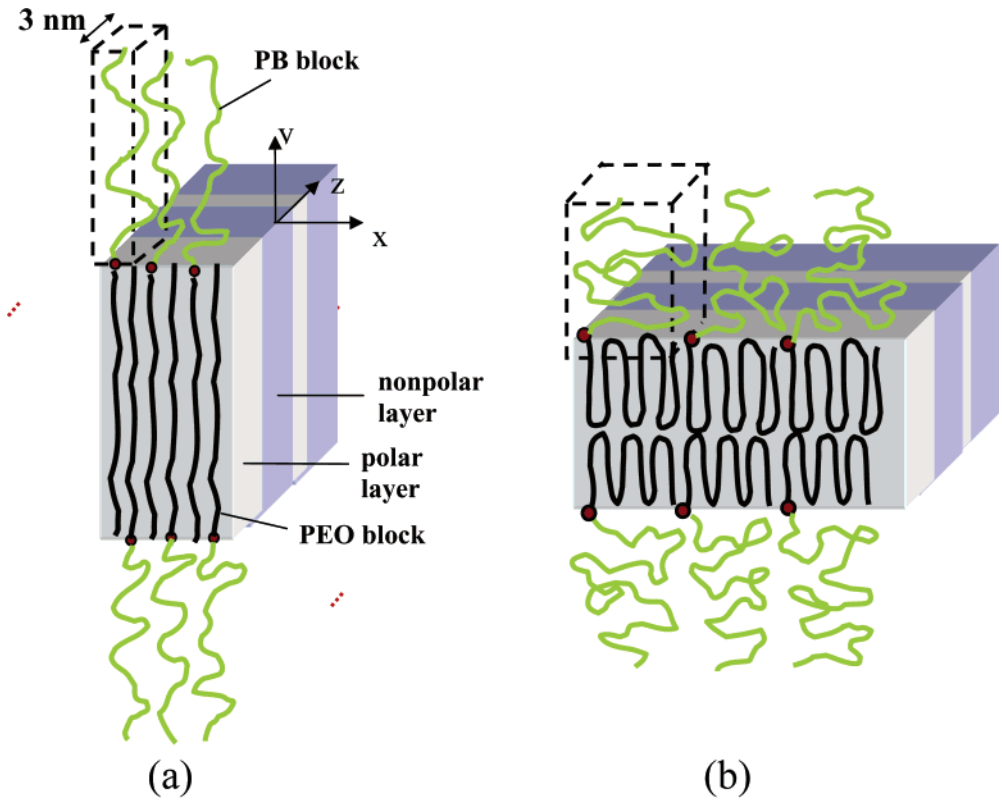

Figure 3. Conformations of PB and DBSA-bound PEO blocks in the case that the PEO(DBSA)$_x$ blocks form a lamellar mesophase. The PEO chains laying on the lamellar plane in (a) are highly stretched normal to the copolymer domain interface. In this case, the conformational freedom of PB blocks in the x direction becomes restricted under the condition of melt incompressibility and hence causes a loss of conformational entropy. The entropic loss can be alleviated if the PEO chains lying on the lamellar plane adopt some folded conformations, as illustrated in (b).

stretching (and hence conformational entropy loss) of the amorphous blocks.[20,21] Consequently, an elastic force due to the conformational entropy loss of PB blocks exists to resist the formation of lamellar mesophase in the PEO(DBSA)$_x$ domain. Such an elastic force is absent in the homopolymer complex, but its presence in the comb−coil diblock may lower T_{ODT} of the lamellar mesophase organized by the comb blocks.

Larger Scale Domain Morphology of PB-*b*-PEO-(DBSA)$_x$. SAXS and TEM are employed to reveal the microdomain structure formed by the PB coil blocks as a function of binding fraction in the PEO(DBSA)$_x$ comb block and temperature. Figure 4 displays the temperature-dependent SAXS profiles in the low-q region (0.1 nm^{-1} < q <1.0 nm^{-1}) for characterizing the PB domain structure. We start our discussion from the sample with $x = 1$ (i.e., the stoichiometric composition), in which the overall volume fraction of the PB block, f_{PB}, is 0.11. According to the classical phase diagram of diblock copolymer, this volume fraction should prescribe a morphology of bcc packed PB spheres dispersed in the matrix constituting the comb blocks.[5,6] However, the corresponding SAXS profiles at 25−50 °C in Figure 4a are not consistent with the scattering patterns from this type of structure. First, the scattering profiles display a single low-q interference peak corresponding to an interdomain distance of 35 nm rather than a series of diffraction peaks characteristic of the bcc lattice, indicating the lack of long-range order of the PB microdomains. Moreover, the relative position (1:1.68) of the two form factor maxima (marked by "$i = n$", $n = 1, 2$) does not follow that ($q_{m,i=1}$:$q_{m,i=2}$ = 5.765:9.095) prescribed by the sphere form factor but instead more closely agrees with that predicted by the cylinder form factor ($q_{m,i=1}$:$q_{m,i=2}$ = 4.98:8.364).[22]

To verify the cylindrical geometry of PB domains, we fit the observed scattering profiles in the q region away from the low-q peak using the polydisperse cylinder form factor. For a system consisting of cylindrical particles with polydisperse radii, R, and constant length, L, the SAXS intensity can be approximated as[23−25]

$$I(q) = N\Delta\rho^2 \int_0^\infty p_R(R)\, P(q,R,L)\, S(q,R)\, \mathrm{d}R \qquad (1)$$

where N is the total number density of the particles, $\Delta\rho$ is the scattering length density difference between the matrix and the particle, $P(q,R,L)$ is the form factor of cylinder describing the intraparticle effect with R and L being the radius and length of the cylinder, respectively, $p_R(R)$ is the normalized probability function expressing the distribution of R, and $S(q,R)$ is the structure factor which describes the interparticle interaction and is related to the spatial arrangement of the particles. The cylinder form factor is given by

$$P(q,R,L) = \int_0^{\pi/2} f^2(q,\alpha) \sin\alpha \, \mathrm{d}\alpha \qquad (2)$$

$$f(q,\alpha) = 2 \cdot V_{cyl} \cdot j_0\left(\frac{qL}{2}\cos\alpha\right) \frac{j_1(qR\sin\alpha)}{(qR\sin\alpha)} \qquad (3)$$

where $j_0(x) = \sin x/x$, $j_1(x)$ is the first-order Bessel function, $V_{cyl} = \pi R^2 L$ is the cylinder volume, and α is the angle between the cylinder axis and the scattering vector, q. The integral in eq 2 signifies an average over

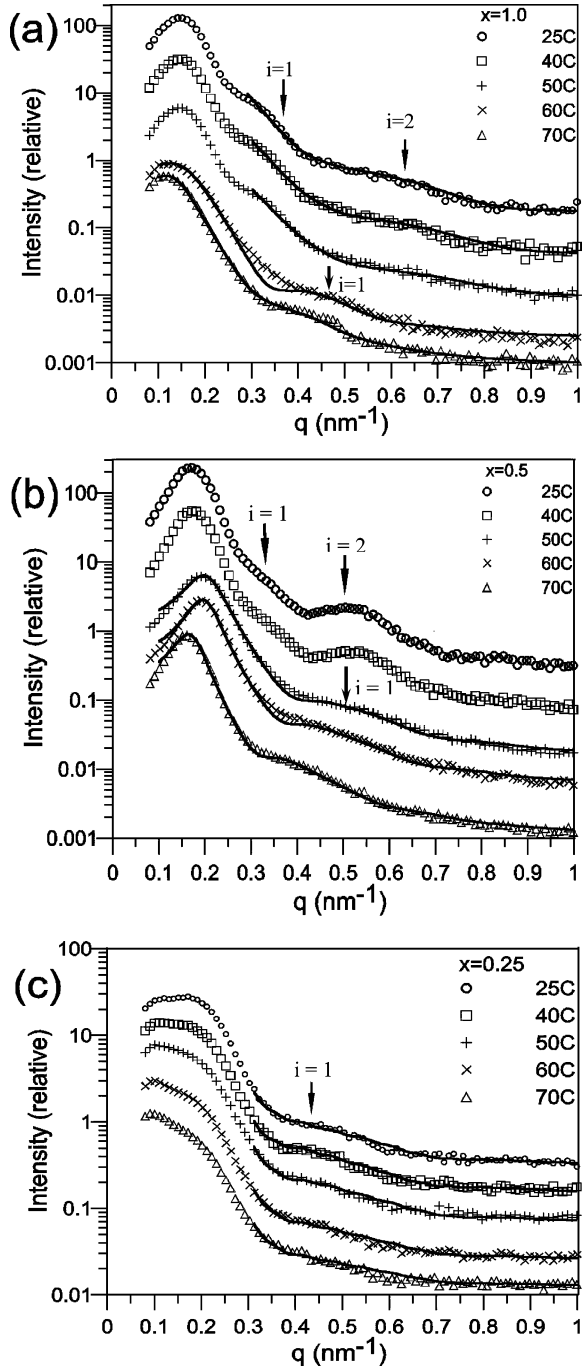

Figure 4. Temperature-dependent SAXS profiles in the low-q region (0.1 $nm^{-1} < q < 1.0$ nm^{-1}) for characterizing the PB domain structure in PB-*b*-PEO(DBSA)$_x$ with x of (a) 1.0, (b) 0.5, and (c) 0.25. The solid curves represent the fits by the polydisperse cylinder form factor or the polydisperse hard-sphere models (see text).

all possible orientations of the cylinder with respect to q. A square size distribution ranging from $R_c(1 - \sigma)$ to $R_c(1 + \sigma)$ is assumed for $p_R(R)$ with σ defined as the ratio of the half-width of square size distribution to the mean radius R_c.

In the present system, the microdomain arrangement is a kind of short-range order, producing a single broad structure factor peak in the SAXS profile. The Percus–Yevick hard-sphere (HS) model has been shown to describe the structure factor associated with this kind of disordered packing well for a wide spectrum of systems.[23–26] In the system containing cylindrical particles, however, the HS model may not be applicable because the volume (of the sphere) enclosed by the rotation of individual cylinder over all orientations overlaps with one another, which contradicts the impenetrable characteristic of hard sphere. Therefore, fitting the entire scattering profiles in Figure 4a using the HS + cylinder form factor model is implausible. Nevertheless, considering that $I(q)$ in the q region away from the structure factor peak (q_{max}) may be well approximated by the form factor $P(q)$ since $S(q,R)$ easily approaches 1.0 at $q > q_{max}$,[25] it is hence justifiable to fit the observed scattering profile in this region using cylindrical form factor alone. It is further noted that in the middle q region (0.3 $nm^{-1} < q < 1.0$ nm^{-1} for the present system) the cylinder form factor profile is predominantly determined by the polydisperse radius rather than the length of the cylinder; consequently, $I(q)$ in this region was fitted by eq 1 with the assumptions of $S(q,R) \approx 1.0$ and $L = \infty$.

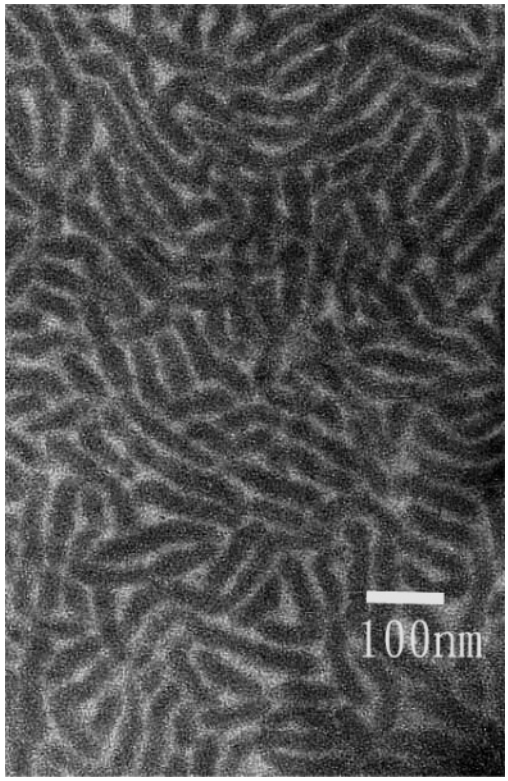

Figure 5. TEM micrograph of PB-*b*-PEO(DBSA)$_{1.0}$ showing the disordered arrangement of cylindrical PB domains with a radius of ca. 14 nm.

The SAXS intensities calculated by the form factor fitting are shown by the solid curves in Figure 4a. It can be seen that cylinder form factor fits the experimentally observed form factor profiles well. The mean cylinder radius deduced from the fitting is ca. 13.5 nm with the corresponding polydispersity parameter σ of 0.46, 0.49, and 0.52 for temperatures of 25, 40, and 50 °C, respectively. This fitting result also demonstrates how the form factor peaks are smeared or broadened by the polydispersity of the radius compared to the well-separated peaks from the monodisperse system.

The microdomain morphology deduced from SAXS is also consistent with the corresponding TEM observation showing disordered arrangement of cylindrical domains with an average radius of ca. 14 nm presented in Figure 5. Therefore, PB-*b*-PEO(DBSA)$_{1.0}$ exhibits a cylinder-

within-lamellae morphology, in which the cylindrical PB domains with the radius of ca. 14 nm are dispersed in a lamellar mesophase with the characteristic length of ca. 3 nm organized by the PEO(DBSA)$_{1.0}$ comb blocks. It is noted that in a PS-*b*-P4VP(PDP)$_{1.0}$ supramolecular comb−coil diblock exhibiting cylinder-within-lamellae morphology the PS cylindrical domains were found to pack in a hexagonal macrolattice,[2] in contrast to the disordered arrangement of PB cylinders observed here. The lack of long-range order of PB domains may be attributed to the strong thermal fluctuation effect (known to disturb the ordered packing of block copolymer microdomains), considering the large mobility of PB and PEO at the temperatures studied due to their very low T_gs (which are more than 150 °C lower than the T_gs of PS and P4VP).

The observed PB domain structure is not consistent with the prediction from the classical phase diagram of coil−coil diblocks because the conformation of the comb blocks forming the lamellar structure greatly deviates from random coil. In this case, the cylindrical microdomain is favored over the spherical one considering that it is easier for the PEO(DBSA)$_x$ lamellar array around a PB cylinder to extend over a long-range once the polar/nonpolar layers stack along the cylinder length direction.

It is further noted that the interdomain distance of the PB cylinders calculated from the primary SAXS peak is about 35 nm. The half of this length is obviously smaller than the fully extended length of the PEO chain with the molecular weight of 11 000 (which is ca. 69 nm). This means that the coronal PEO chains confined between the polar layers are not fully stretched normal to the domain interface but rather adopt some folded conformation to alleviate the entropic penalty of PB blocks (cf. Figure 3b).

As the temperature increases to 60 °C, the SAXS profile in Figure 4a undergoes an abrupt change characterized by the shifts of the primary peak and the first-order form factor maximum to lower and higher q, respectively. Interestingly, this change of scattering pattern occurs concurrently with the ODT of the PEO(DBSA)$_{1.0}$ comb block (cf. Figure 1a), signaling the disruption of the lamellar structure of the comb blocks perturbed the morphology of PB domain concurrently. This is understandable considering that PB-*b*-PEO(DBSA)$_x$ may be simply regarded as a mixture of a diblock copolymer with a DBSA selective solvent when the comb block is in the disordered state. In this case, spherical domain becomes the favored structure for the PB block judging from its volume fraction of 0.11. The corresponding SAXS profiles at $T \geq 60$ °C are hence associated with the spherical PB domains dispersed in a disordered matrix of PEO(DBSA)$_{1.0}$ blocks. These spherical domains are also disorderly arranged considering that only a broad primary scattering peak is observed at low q.

To verify the disordered sphere morphology at $T \geq 60$ °C, the corresponding SAXS profiles are fitted by the Percus−Yevick[26] hard-sphere theory assuming the liquidlike packing of hard-sphere domains. The hard-sphere radius, R_{HS}, adopted here covers an impenetrable shell corresponding to the coronal layer surrounding the spherical domain and is related to the actual domain radius, R, by a constant C_{HS}, viz. $R_{HS} = C_{HS}R$, according to Kinning et al.[23] The model used here also incorporates the polydispersity effect by assuming a Schultz size distribution.[27] In this case, the SAXS intensity is written as

$$I(q) = N\Delta\rho^2 \int_0^\infty p(R)\, P(q,R)^2\, S(q,R_{HS},\eta_{HS})\, dR \quad (4)$$

where $p(R)$ is the Schultz size distribution in normalized form for the polydispersed domains. The polydispersity term describing the width of a given size distribution is defined herein as the ratio of the variance of the Schultz size distribution to the mean radius. $P(q,R)^2$ is the form factor of a spherical domain expressed as

$$P(q,R) = 4\pi R^3 \cdot \left[\frac{\sin(qR) - (qR)\cos(qR)}{(qR)^3}\right] \quad (5)$$

$S(q,R_{HS},\eta_{HS})$ is the interparticle structure factor for hard-sphere model and is related to the interference peak in the SAXS profile. The term η_{HS} is the volume fraction of the hard spheres. $S(q,R_{HS},\eta_{HS})$ using the Percus−Yevick expression is given by[23−25]

$$S(q,R_{HS},\eta_{HS}) = \frac{1}{1 + 24\eta_{HS}(G(A)/A)} \quad (6)$$

where $A = 2qR_{HS}$ and

$$G(A) = \frac{\alpha}{A^2}(\sin A - A\cos A) + \frac{\beta}{A^3}[2A\sin A + (2 - A^2)\cos A - 2] + \frac{\gamma}{A^5}\{-A^4\cos A + 4[(3A^2 - 6)\cos A + (A^3 - 6A)\sin A + 6]\} \quad (7)$$

$$\alpha = (1 + 2\eta_{HS})^2/(1 - \eta_{HS})^4 \quad (8)$$

$$\beta = -6\eta_{HS}(1 + \eta_{HS}/2)^2/(1 - \eta_{HS})^4 \quad (9)$$

$$\gamma = \frac{1}{2}\eta_{HS}(1 + 2\eta_{HS})^2/(1 - \eta_{HS})^4 \quad (10)$$

Table 2. Parameters Obtained by the Polydisperse Hard-Sphere Model Fitting of SAXS Data

x	T (°C)	av radius $\langle R\rangle$ (nm)	polydispersity	$C_{HS} = R_{HS}/R$
1.0	60	12.5	0.145	1.42
1.0	70	13.4	0.189	1.52
0.5	50	10.8	0.144	1.39
0.5	60	11.4	0.145	1.37
0.5	70	13.3	0.155	1.35

Table 2 lists the average radius of PB spherical domain, polydispersity of size distribution, and C_{HS} obtained from the model fit. The SAXS intensities calculated by this model analysis (cf. solid lines in Figure 4a) agree well with the measured data. The average radius of the spherical domains is seen to increase with increasing temperature, as also manifested from the shift of the first-order form factor maximum (marked by "$i = 1$") to lower q as the temperature increases in Figure 4a. This reveals that a portion of DBSA molecules decouple from PEO backbone and diffuse into the PB domains due to decrease of selectivity of DBSA toward PEO with increasing temperature.

The temperature effect on the SAXS profile for the binding fraction of $x = 0.5$ is virtually the same as that observed for $x = 1.0$, where the scattering pattern undergoes a sudden change across the ODT of the PEO-$(DBSA)_{0.5}$ comb block (cf. Figure 4b). The SAXS profiles at 25−40 °C at which the PEO$(DBSA)_{0.5}$ blocks form lamellar mesophase signal a disordered arrangement of cylindrical PB domains. Because f_{PB} of this sample (=0.20) is higher than that associated with $x = 1.0$, cylindrical domains with a larger radius are formed, making the form factor peaks (marked by "$i = n$", $n = 1, 2$) locate at lower q compared with those observed in Figure 4a. It is noted that the first-order peak of the cylinder form factor appears at a position close to the interference peak, and its amplitude is reduced due to overlap with the valley damping[25] of the structure factor characterizing the disordered arrangement of the cylinders. Because of such a convolution effect, it is implausible to fit the observed form factor profiles using cylinder form factor alone. Nevertheless, the relative position of the two observed form factor peaks (i.e., 0.31 nm^{-1}:0.51 nm^{-1}) agrees with that prescribed by the cylindrical form factor (i.e., 4.98:8.364). The radius of the PB cylinders estimated from the peak position is ca. 16.4 nm.

The SAXS profiles at 50−70 °C (i.e., above the T_{ODT} of PEO$(DBSA)_{0.5}$) are very similar to those of $x = 1$ exhibiting the morphology of disorderly arranged spherical PB domains (i.e., the profiles at $T \geq 60$ °C in Figure 4a). Therefore, the ODT of the comb blocks also induces a concurrent transformation of the PB domain morphology into disordered spheres. The first-order peak of the sphere form factor (marked by "$i = 1$") also shifts to lower q with increasing temperature, indicating that the domain radius increases accordingly due to the diffusion of DBSA into the PB domains. The solid curves in Figure 4b represent the fits by the polydisperse hard-sphere model (i.e., eq 4). The average radii of the spherical domains at different temperatures derived from the fit are also tabulated in Table 2.

Figure 4c displays the temperature-dependent SAXS profiles for the composition of $x = 0.25$ which prescribes the f_{PB} of 0.28. In contrast to the $x = 0.5$ and 1.0, this sample exhibits similar scattering pattern in terms of the position of the form factor maximum over the temperature range studied, showing the preservation of PB domain morphology with respect to temperature change. According to Figure 1c, PEO$(DBSA)_{0.25}$ blocks are always in the disordered state over the temperature range studied; therefore, PB-*b*-PEO$(DBSA)_{0.25}$ behaves like a diblock copolymer/selective solvent mixture. In this case, the PB block should self-assemble to form cylindrical microdomains judging from its volume fraction of 0.28. At 25 °C the single broad interference peak demonstrates that these cylindrical domains are also disorderly arranged. The corresponding form factor peaks are however broader and less discernible than those exhibited by the other two samples with higher DBSA binding fractions, indicating that the cylinders are more distorted. The more distorted cylinders are confirmed by the TEM micrograph in Figure 6, showing the morphology of PB domains at room temperature. The solid curves in Figure 4c represent the fits by the polydisperse cylinder form factor (i.e., eq 1). The mean radius of the cylindrical domains obtained from the fits is ca. 11.6 nm and is consistent with that estimated from the TEM micrograph. It is worth noting that the low-q interference peak broadens or even vanishes at higher temperatures ($T > 40$ °C). This appears to suggest that the microphase separation between PEO$(DBSA)_{0.25}$ comb blocks and PB coil blocks starts to be suppressed at a temperature far below the ODT of neat PEO-*b*-PB ($T_{ODT} > 200$ °C). Consequently, binding DBSA onto PEO blocks effectively lowers the segregation strength between PEO and PB and hence reduces the microphase transition temperature significantly.

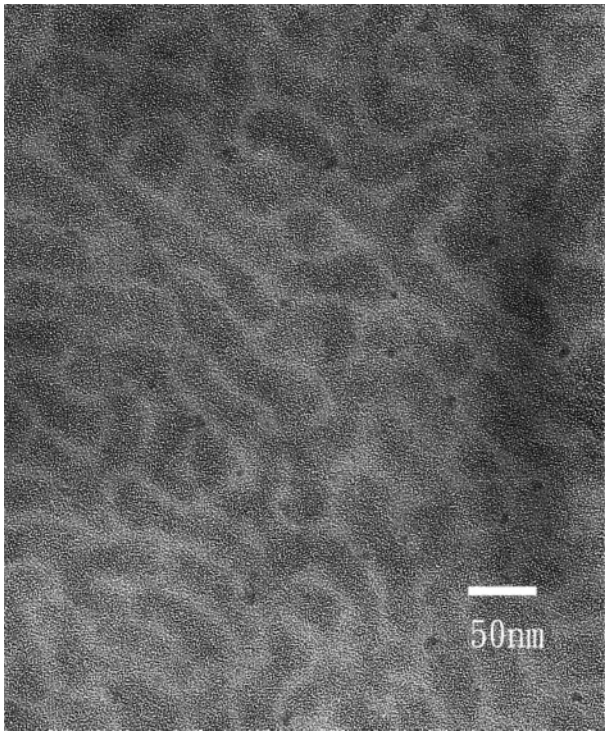

Figure 6. TEM micrograph of PB-*b*-PEO$(DBSA)_{0.25}$ showing the disordered arrangement of distorted PB cylinders.

Conclusions

The phase behavior of a supramolecular comb−coil diblock copolymer formed by binding DBSA onto the PEO block in a PB-*b*-PEO through hydrogen bonding has been investigated. For the binding fractions studied, PB-*b*-PEO$(DBSA)_x$ exhibited a *PB* cylinder-within-PEO-$(DBSA)_x$ lamellae morphology, except for the low binding fraction of $x = 0.25$ in which the comb blocks were in the disordered state. Rather than fully stretched normal to the interface of the PB cylinder, the PEO blocks confined within the polar layers in the PEO-$(DBSA)_x$ lamellar mesophase adopted a folded conformation to alleviate the entropic penalty of the PB blocks while accommodating the formation of lamellar stacks. The ODT of the PEO$(DBSA)_x$ blocks was found to occur at moderate temperatures (45−55 °C), and this transition induced a concurrent transformation of the larger scale PB domain morphology from cylinder to sphere. Consequently, the present system exhibited a structure-within-structure morphology below the T_{ODT} of the comb block and a transition-driven-transition process where the ODT of the smaller scale assembly induced a morphological transformation of the larger scale copolymer domain.

Acknowledgment. This work was supported by the National Science Council of R.O.C. under Grant NSC 92-2216-E-110-009.

References and Notes

(1) Muthukumar, M.; Ober, C. K.; Thomas, E. L. *Science* **1997**, *277*, 1225.
(2) Ruokolainen, J.; ten Brinke, G.; Ikkala, O. *Adv. Mater.* **1999**, *11*, 777.
(3) Ruokolainen, J.; Mäkinen, R.; Torkkeli, M.; Mäkelä, T.; Serimaa, R.; ten Brinke, G.; Ikkala, O. *Science* **1998**, *280*, 557.
(4) Mäki-Ontto, R.; de Moel, K.; Polushkin, E.; van Ekenstein, G. A.; ten Brinke, G.; Ikkala, O. *Adv. Mater.* **2002**, *14*, 357.
(5) Bates, F. S.; Fredrickson, G. H. *Annu. Rev. Phys. Chem.* **1990**, *41*, 525.
(6) Leibler, L. *Macromolecules* **1980**, *13*, 1602.
(7) Chen, H.-L.; Lin, S.-Y.; Huang, Y.-Y.; Chiu, F.-C.; Liou, W.; Lin, J. S. *Macromolecules* **2002**, *35*, 9434.
(8) Antonietti, M.; Wenzel, A.; Thünemann, A. *Langmuir* **1996**, *12*, 2111.
(9) Ikkala, O.; Ruokolainen, J.; ten Brinke, G.; Torkkeli, M.; Serimaa, R. *Macromolecules* **1995**, *28*, 7088.
(10) Antonietti, M.; Conrad, J.; Thünemann, A. *Macromolecules* **1994**, *27*, 6007.
(11) Chen, H. L.; Hsiao, M. S. *Macromolecules* **1999**, *32*, 2967.
(12) Ruokolainen, J.; ten Brinke, G.; Ikkala, O.; Torkkeli, M.; Serimaa, R. *Macromolecules* **1996**, *29*, 3409.
(13) Ruokolainen, J.; Torkkeli, M.; Serimaa, R.; Komanschek, B. E.; Ikkala, O.; ten Brinke, G. *Phys. Rev. E* **1996**, *54*, 6646.
(14) Ruokolainen, J.; Tanner, J.; Ikkala, O.; ten Brinke, G.; Thomas, E. L. *Macromolecules* **1998**, *31*, 3532.
(15) Ruokolainen, J.; Torkkeli, M.; Serimaa, R.; Komanschek, B. E.; ten Brinke, G.; Ikkala, O. *Macromolecules* **1997**, *30*, 2002.
(16) Tal'roze, R. V.; Kuptsov, S. A.; Sycheva, T. I.; Bezborodov, V. S.; Platé, N. A. *Macromolecules* **1995**, *28*, 8689.
(17) Ruokolainen, J.; Saariaho, M.; Ikkala, O.; ten Brinke, G.; Thomas, E. L.; Torkkeli, M.; Serimaa, R. *Macromolecules* **1999**, *32*, 1152.
(18) Chen, H. L.; Ko, C. C.; Lin, T. L. *Langmuir* **2002**, *18*, 5619.
(19) Rädler, J. O.; Koltover, I.; Salditt, T.; Safinya, C. R. *Science* **1997**, *275*, 810.
(20) DiMarzio, E. A.; Guttman, C. M.; Hoffman, J. D. *Macromolecules* **1980**, *13*, 1194.
(21) Whitmore, M. D.; Noolandi, J. *Macromolecules* **1988**, *21*, 1482.
(22) Hashimoto, T.; Fujimura, M.; Kawai, H. *Macromolecules* **1980**, *13*, 1660.
(23) Kinning, D. J.; Thomas, E. L. *Macromolecules* **1984**, *17*, 1712.
(24) Tsao, C. S.; Lin, T. L. *J. Appl. Crystallogr.* **1999**, *32*, 426.
(25) Pedersen, J. S. *J. Appl. Crystallogr.* **1994**, *27*, 595.
(26) Percus, J. K.; Yevick, G. J. *Phys. Rev.* **1958**, *110*, 1.
(27) Hayter, J. In *Physics of Amphiphiles-Micelles, Vesicles and Microemulsions*; DeGiorgio, V., Corti, M., Eds.; Elsevier: North Holland, 1983; p 69.

MA048526H